

Analysis of the Rotary-draw Bending Process for Thin-walled Rectangular Aluminum Tube

S. M. Seyyedhatami and H. Lexian*

Faculty of Material & Manufacturing Technologies, Malek Ashtar University of Technology, Tehran, Iran

ARTICLE INFO

Article history:

Received 21 June 2019
Revised 23 November 2019
Accepted 26 December 2019

Keywords:

Rotary-draw bending
Rectangular cross sections
Analytical analysis
Power law hardening model

ABSTRACT

The Rotary-Draw Bending (RDB) process is a distinguished process employed for the precision cold bending of a hollow tube with small radius bends using Numerical Control (NC) machines. This research presents an analytical model based on the power law hardening model for the RDB processing of rectangular thin tubes. Based on the constraints of the tube in the dies and its thinness, the plane stress assumption in the thickness direction and the plane strain assumption in the transverse direction for all faces of the tube are used. By assuming the proportionality of the process and using the Levy–Mises flow rule hypothesis, the stress field of the tube is predicted and the balance of the forces in all aspects of the tube is used to identify the position of the neutral axis. Then the bending moment as well as the amount of the spring back is developed analytically. By analyzing the geometry of the tube and the process, a new mandrel is designed and constructed. The process has been modeled and analyzed using the explicit finite element ABAQUS commercial code and also carried out experimentally. Comparison of the analytical, numerical and experimental strain fields shows good agreement.

© Shiraz University, Shiraz, Iran, 2020

Nomenclature

A	Area
a	Width of the tube
b	Height of the tube
E	Elastic modulus
h_1	Position of bending natural axis of the section relative to the external face
I	Second moment of area
K	Strain hardening coefficient
K	$(2/\sqrt{3})^{n+1} K$
M	Pure bending moment
n	Strain hardening power
R	Bending radius
\bar{R}	Average bending radius
T	Circumferential stress resultant force
t_0	Initial thickness
T_{total}	Total circumferential stress resultant force
α	a/b
$\Delta\theta$	Amount of spring back
ε	Strain
$\bar{\varepsilon}$	Equivalent strain
η	h_1/b
θ	Angle of bending
ρ	R/b
$\bar{\sigma}$	Equivalent stress
σ	Stress

τ	t_0/b
χ	r/b
Subscript	
e	External side of the cross section
i	Internal side of the cross section
l	Lateral side of the cross section
r	Radial direction
t	Tangential direction
$total$	Total force
z	Axial direction

1. Introduction

Due to their high quality in transmitting electrical signals, low weight and good vibration absorption capability, aluminum cross sections are widely used in aviation, aerospace, satellite ground stations, radars, etc [1]. Bending process of these cross sections is based on the theory of a large and sufficient force used for creating a tension beyond the elastic limit of the material which should not exceed the ultimate strength of the material; otherwise, it will lead to workpiece failure [2].

* Corresponding author
E-mail address: lexian@mut.ac.ir (H. Lexian)

By the middle of the twentieth century, bending profiles with rectangular cross sections for microwave equipment were so hard and costly, resulting in their slow improvement. Later, with an increase in aerospace equipment, the need for the bending techniques became much more considerable. Therefore, nowadays, applying a process by which uniform products with closed tolerances can be produced in a limited period of time is considered to be an important matter in profile bending.

Four prevalent methods are used in profile bending with rectangular cross sections: rolling, stretch, compression, and drawing. Choice of the method depends on the number of components, profile dimensions, wall thickness, profile material, radius and the number of bends in addition to the required accuracy, the determined quality, and the available facilities [3]. In addition to the above-mentioned methods, rotary-draw bending, which is called RDB, is a new method. Apart from being economical, it is a unique method for bending small radiuses in a rectangular cross section profile with thin walls.

Rotary-draw bending which is used for the accurate bending of such kinds of profiles with thin walls in NC numerical systems, has a major functionality in leading industries such as aviation, aerospace, radars, and satellite communications [4]. Using this process in bending, such kinds of profiles with electromagnetic wave transmission lines will decrease the costs. It also leads to an increase in the quality and uniformity of the products [5, 6].

Rotary draw bending process is a plastic geometry deformation process with nonlinear material behavior and nonlinear boundary conditions. It has numerous effective parameters which deform large strains and cause failures in the workpiece. In recent years, the bending rectangular cross section profile has been studied widely in different papers. Most of them focus more on the stretch bending process and less on the rotary draw bending process [7].

Rotary draw bending process has four dies: Bending Die, Wiper Die, Pressure Die, and Clamp Die which can be observed in Fig. 1. In the bending process, the rectangular cross section profile is placed in the inner

canal of the wiper die; and the clamp die holds the profile against the bending die. When the profile rotates around the bending die, the pressure die makes a linear movement along the profile and stops the rotating profile. The process ends when the bending angle reaches the desirable size.

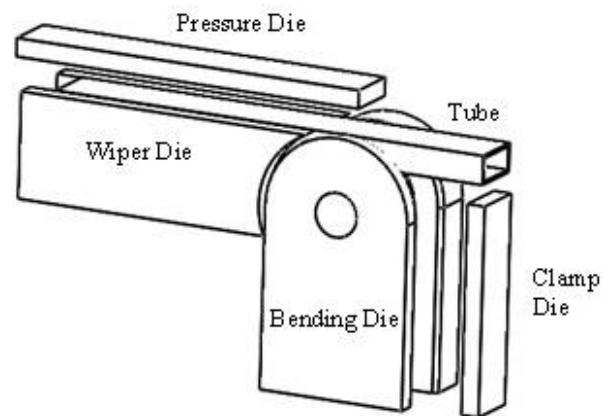


Fig. 1. Different dies in the rotary draw bending process.

Liu et al. [8], in a numerical experimental research based on the distortion ratio of the cross sections, evaluated the effects of different die parameters on this ratio. Their results indicated that with the increase of the bend radius, the clamp pressure, the number of mandrel cores and the distortion ratio decrease. On the other hand, the increase of the bend speed and angle, the increase of the protrusivity of the mandrel, and the increase of the clearance between the profile and the pressure die will lead to the increase of this ratio. Furthermore, the effects of the bending die and mandrel cores on the cross section are important factors, while the effects of the clamp die and pressure die are minimal [8].

Tian et al. [9], evaluated the effects of the geometrical ratios with rectangular cross sections in the wrinkling phenomenon. By defining the maximum height of the wrinkling wave of the inner arch and the side wrinkling of the bend, they concluded that the increase in the height and width of the rectangular cross section profile leads to the increase of the maximum height of the wrinkling wave in the inner arch and the side wrinkling of the bend. Furthermore, the increase in

the ratio of the bending radius to the height of the rectangular cross section profile leads to a decrease in the height of the wrinkling wave of the inner arch and the side wrinkling of the bend. This research with bending ratio of 2.87 on aluminum profiles does not focus on the geometrical dies [9].

Xing et al. [10], in his research, simulated the process and analyzed the distribution of stress and strain along with the variations in the profiles' wall thickness (profiles with steel rectangular cross sections with bend radiuses of 75, 90, 105, and 120 mm). It was indicated that the increase in the bending radius led to the increase of the formability properties and reduced the tendency toward wrinkling and rupture [10].

Shen et al. [11] used the FE model (which belongs to profile deformation with rectangular cross sections) and proposed three sections, including mandrels, clamp die, and the middle section. They calculated the relationship between the distortions of the cross sections and stress components. The maximum cross section distortion in the up and down dimensions of the profile is in the symmetry line, and in the side dimensions it is in the corner of the profile [11]. In the above-mentioned study, there can be seen no reference to the mandrel and die design. The experiments were carried out on the aluminum rectangular cross sections with the ratio of 2.5.

With regard to the analytical models to analyze the process, the following researches can be noted. The important factor in determining the quality of RDB bending is the collapsing deformation of the thin-walled rectangular tube. Liu et al. [4] presented an analytical model for collapsing deformation, showing that among the elements of the process, the clamp die and cores of mandrel had a greater impact on collapsing deformation [4].

Paulsen et al. [12] presented an analytical model to determine the local post-buckling and suck-in deformations in the rectangular tube bending based on the deformation theory of plasticity combined with the energy method. However, the model is not suitable to predict the large local deformation and the large displacement in the rotary-draw bending process due to the localization of the post-buckling deformation [12].

In this study, an analytical model based on the power law hardening model is presented to analyze the stresses, strains and moments in the rotary-draw bending process for the thin-walled rectangular tube. The balance of the forces in all aspects of the tube is used to identify the position of the neutral axis. Then, the strains, stresses and bending moments are extracted, and the spring back is predicted. In all of the above studies, the bending ratio (bend radius of the inner arch to the profile height) is 2.5, 2.87, 3.28, etc. and there is no reference to the die and mandrel designs. The reduction in the bend radius will increase the forces and the probability of the failure in the mandrel cores.

The purpose of this study is to successfully coagulate a hollow aluminum cross section with a bending ratio of 1.6. Due to the small bending ratio, the possibility of wrinkling or rupture of the workpiece is so high. Therefore, the first and most important challenge in this matter is to set a correct design, and the reduction of the failures in the mandrel cores. In this study, a new core geometry is presented whose design was based on the relationships extracted from this paper. At the end, it leads to the successful implementation of the process.

2. Analysis of RDB Process

In this study, an analytical model based on the strain hardening power law is used to analyze the RDB process. It is assumed that the directions of the coordinate axis shown in Fig. 2 are the principle stress directions.

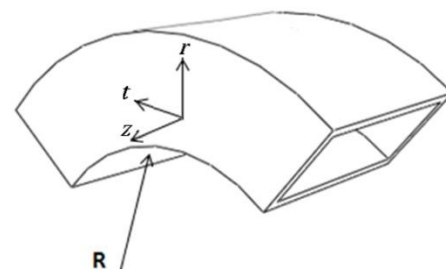


Fig. 2. Coordinate axis of the bent.

As the pure bending moment M is used for bending the tube and neglecting frictional forces, the total circumferential stress resultant force of any cross-section of the tube along the bent must be equal to zero. Therefore, it can be written as:

$$T_{total} = \int_{A_c} \sigma_r dA = \int_{A_e} \sigma_{et} dA + \int_{A_i} \sigma_{it} dA + 2 \int_{A_l} \sigma_{lt} dA = T_e + T_i + 2T_l = 0 \quad (1)$$

Where A_c is the total cross section area and A_e , A_i , and A_l are areas of the external side, internal side and lateral side of the cross section, respectively as shown in Fig. 3.

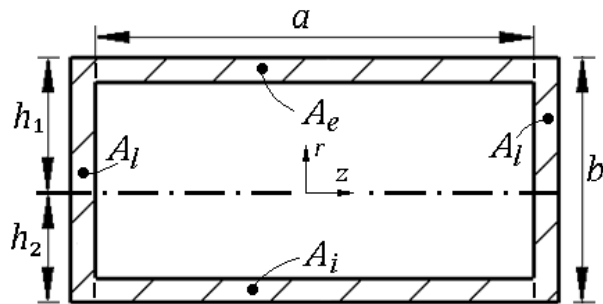


Fig. 3. Cross section of the tube.

Due to the small thickness of the tube, the plane stress assumption is used in the thickness direction. Furthermore, due to the rigid core inside the tube, plane strain assumption can be used in r and z directions for the lateral and external-internal faces, respectively.

In this research, regardless of the elastic zone, a power law strain hardening model is used for material behavior:

$$\bar{\sigma} = K \bar{\varepsilon}^n \quad (2)$$

Where K is the strain hardening coefficient, and the equivalent stress, $\bar{\sigma}$, and the equivalent strain, $\bar{\varepsilon}$, are defined as:

$$\bar{\sigma} = \sqrt{\frac{1}{2} [(\sigma_r - \sigma_t)^2 + (\sigma_t - \sigma_z)^2 + (\sigma_r - \sigma_z)^2]} \quad (3)$$

$$\bar{\varepsilon} = \sqrt{\frac{2}{3} (\varepsilon_r^2 + \varepsilon_t^2 + \varepsilon_z^2)} \quad (4)$$

The assumption of the plane strain in z direction and the use of the incompressibility condition, cause the strain filed of the external face of the bent to be:

$$\varepsilon_{ez} = 0, \varepsilon_{er} = -\varepsilon_{et} \quad (5)$$

The assumption of the plane stress in r direction and proportionality of the process, and the use of the hypothesis of the Levy-Mises flow rule, cause the stress filed of the external face to be:

$$\sigma_{er} = 0, \sigma_{ez} = \frac{1}{2} \sigma_{et} \quad (6)$$

Substituting equations (5) and (6) in (4) and (3), respectively and the results in Eq. (2), we can write:

$$\sigma_{et} = \left(\frac{2}{\sqrt{3}} \right)^{n+1} K \varepsilon_{et}^n = \dot{K} \varepsilon_{et}^n \quad (7)$$

Due to the small thickness of the tube compared to its height, a uniform tangential strain in the external face can be assumed and written as:

$$\varepsilon_{et} = \frac{\eta - \tau/2}{1 + \rho - \eta} \quad (8)$$

Where $\eta = h_1/b$, $\tau = t_0/b$, $\rho = R/b$ and h_1 , t_0 , R and b are the positions of the bending natural axis of the section relative to the external face, initial thickness, bending radius and height of the tube, respectively. Substituting Eq. (8) in (7) and the result in Eq. (1), we can write:

$$T_e = at_e \sigma_{et} = at_0 (1 - \varepsilon_{et}) \dot{K} \varepsilon_{et}^n = at_0 K' (\varepsilon_{et}^n - \varepsilon_{et}^{n+1}) \quad (9)$$

In a manner similar to the external face, we can write for the internal face:

$$\sigma_{it} = - \left(\frac{2}{\sqrt{3}} \right)^{n+1} K (-\varepsilon_{it})^n = -\dot{K} (-\varepsilon_{it})^n \quad (10)$$

$$\varepsilon_{it} = \frac{\eta + \tau/2 - 1}{1 + \rho - \eta} \quad (11)$$

$$T_i = at_i \sigma_{it} = -at_0 (1 - \varepsilon_{it}) \dot{K} (-\varepsilon_{it})^n = -at_0 K' ((-\varepsilon_{it})^n + (-\varepsilon_{it})^{n+1}) \quad (12)$$

For the lateral faces, the assumption of the plane strain in r direction and the use of the incompressibility condition cause the strain filed of the lateral faces to be:

$$\varepsilon_{er} = 0, \varepsilon_{ez} = -\varepsilon_{et} \quad (13)$$

The assumption of the plane stress in z direction and proportionality of the process, and the use of the hypothesis of the Levy-Mises flow rule cause the stress filed of the lateral faces to be:

$$\sigma_{ez} = 0, \sigma_{er} = \frac{1}{2} \sigma_{et} \quad (14)$$

Substituting equations (13) and (14) in (4) and (3), respectively and the results in Eq. (2), we can reacquire Eq. (7).

Tangential strain in the lateral face can be written as:

$$\varepsilon_{lt} = \frac{\chi}{1 + \rho - \eta} \quad (15)$$

Where $\chi = r/b$ and r is measured from the natural axis

outward the bend as depicted in Fig. 7. Substituting Eq. (15) in (7) and the result in Eq. (1), we can write:

$$T_l = \int_{A_s} \sigma_l dA = \int_{\eta-1}^{\eta} K(1-\varepsilon_{li})(\varepsilon_{li})^n bt_0 d\chi \quad (16)$$

After some cumbersome algebra analyses, the net circumferential resultant force of the lateral side of the section can be written as:

$$T_l = \frac{bt_0 K'}{(1+\rho-\eta)^n} \left(\frac{\eta^{n+1} - (1-\eta)^{n+1}}{n+1} - \frac{\eta^{n+2} + (1-\eta)^{n+2}}{(n+2)(1+\rho-\eta)} \right) \quad (17)$$

Substituting equations (9), (12) and (17) in (1), the total circumferential resultant force of the section can be written as:

$$T_{total} = \frac{bt_0 K'}{(1+\rho-\eta)^n} \left\{ \frac{\alpha \left[(1+\rho-2\eta+\tau/2)(\eta-\tau/2)^n - (2+\rho-2\eta-\tau/2)(1-\eta-\tau/2)^n \right]}{1+\rho-\eta} + 2 \frac{\eta^{n+1} - (1-\eta)^{n+1}}{n+1} - 2 \frac{\eta^{n+2} + (1-\eta)^{n+2}}{(n+2)(1+\rho-\eta)} \right\} = 0 \quad (18)$$

Where $\alpha = a/b$. Eq. (18) can be solved to find the position of the bending natural axis, η , using the Newton-Raphson method. As seen in Eq. (18), the position of the bending natural axis depends only on the aspect ratio, α , thickness ratio, τ , bending ratio, ρ , and the strain hardening power, n .

After finding η , strains and stresses of the bend are acquired, and the pure bending moment can be attained as:

$$M = \int_{A_s} r \sigma_l dA \quad (19)$$

In a similar manner of finding the total circumferential resultant force, the pure bending moment can be acquired as:

$$\frac{M}{b^3 K'} = \alpha \tau \frac{(1+\rho-2\eta+\tau/2)(\eta-\tau/2)^{n+1} + (2+\rho-2\eta-\tau/2)(1-\eta-\tau/2)^{n+1}}{(1+\rho-\eta)^{n+1}} + \frac{2\tau \left[\eta^{n+2} + (1-\eta)^{n+2} \right]}{(n+2)(1+\rho-\eta)^n} + \frac{2\tau \left[(1-\eta)^{n+3} - \eta^{n+3} \right]}{(n+3)(1+\rho-\eta)^{n+1}} \quad (20)$$

After determining the position of the bending neutral axis and moment in the process, the amount of the spring back ($\Delta\theta$) after ending the process and releasing the bending moment can be derived from the bending stress relationship. If we assume that the unloading of the tube

will be an elastic process, then the elastic bending equation can be written as:

$$\sigma = E\varepsilon = E \frac{y}{R} = \frac{My}{I} \quad (21)$$

Differentiation of the last equality of Eq. (21) results in:

$$\frac{E}{R} = \frac{M}{I} \rightarrow E\Delta\left(\frac{1}{R}\right) = \frac{\Delta M}{I} \quad (22)$$

Where ΔM is the bending moment calculated from Eq. (20). The length of the mid-surface of the bending tube is $l = \bar{R}\theta$ and will remain unchanged during the unloading. From this, we obtain:

$$l \frac{1}{R} = \theta \quad (23)$$

Differentiating Eq. (23), in which l is constant, we obtain

$$\Delta\left(\frac{1}{R}\right) = \frac{\Delta\theta}{\bar{R}\theta} \quad (24)$$

Substituting Eq. (24) in (22) results in:

$$\frac{\Delta\theta}{\theta} = \frac{\Delta M \bar{R}}{EI} \quad (25)$$

Where θ is the angle of bending, E is the elastic modulus, $\bar{R} = R + b/2$ is the average bending radius and $I = \left[(a+2t)b^3 - a(b-2t)^3 \right] / 12$ is the second moment of the area.

3. FEM and Numerical Analysis of the Process

In this study, the explicit finite element analysis is used for the numerical study of the RDB process in commercial ABAQUS software which is compared with the implicit method. The explicit finite element analysis is able to simulate complex processes with large deformations and dynamic contact conditions with greater convergence. The bending die, pressure die, clamping die and mandrel and its cores were modeled as 3D rigid bodies. The mandrel and the wiper die were fixed at the reference point, and the clamp and bending dies rotated together at 1.57 radians around the reference point. For all the mandrels and their cores, which were rigid, a four-node element was used. Quadruple shell element was used for the profile. The approximate size of the profile elements was considered to be 2.5 mm, and

therefore, the profile with 2160 four dimensional elements was demolished. The reference point for applying boundary conditions and the loads were defined for all dies. All contacts were defined surface to surface using the penalty method. The friction coefficient of the contact surfaces, based on their type of surface and lubrication, was considered as shown in Table 1, depending on the lubrication type. Fig. 4 depicts the geometry model and finite element model.

Table 1. Contacts in finite element analysis [7]

Contact bodies	Friction coefficient	Lubrication type
Mandrel/cores	0.02	S980B oil
Mandrel/tube	0.02	S980B oil
Clamp die/tube	0.7	dry friction
Others/tube	0.17	10W oil

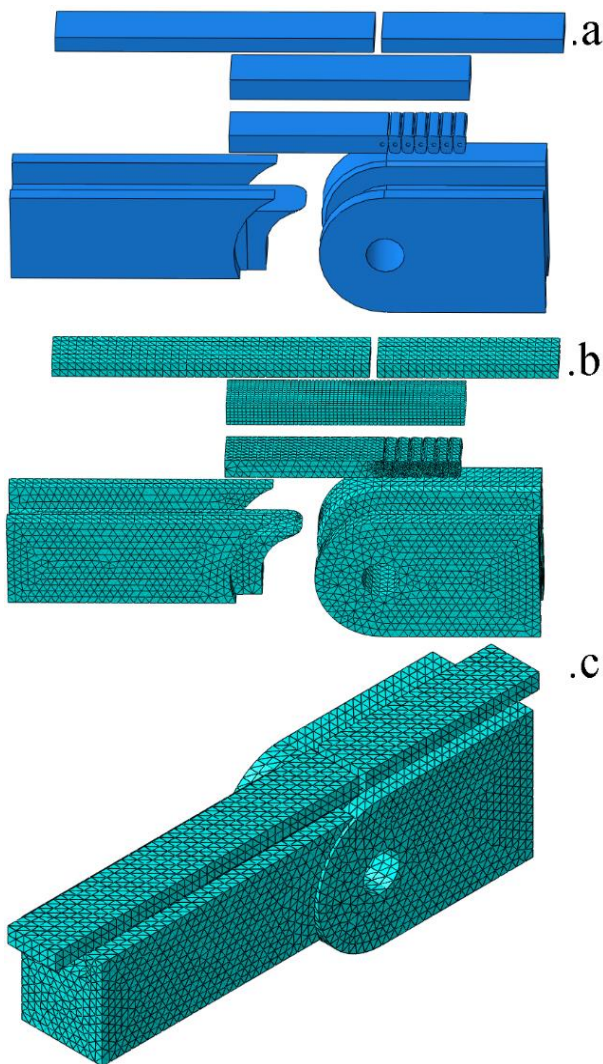


Fig. 4. (a) Geometry model, (b) finite element model and (c) assembled finite element model.

The simulation results also show that in Fig. 5, the end of the process. Moreover, the FEM model of the annealed profile was performed. The main strain contour is shown in Fig. 6.

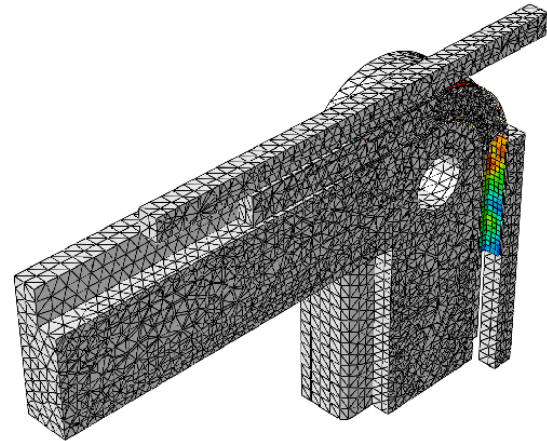


Fig. 5. FEM in the end of the process.

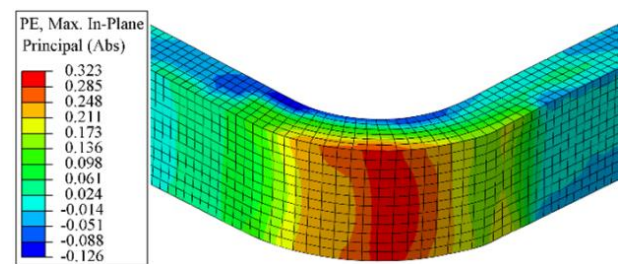


Fig 6. Main strain contour caused by the FEM of the annealed rectangular cross sectional aluminum.

4. The Experimental Study of the Process

Bending die radius was as wide as the arch bend. Wiper die was actually a canal in which the profile was fitted with a suitable clearance and situated in the width direction. Its main role was to prevent wrinkling in the inner arch bend. In this study, the clearance in the width of the profile was 1.5 percent, and the canal height was 3 percent lower than the profile height.

The bending and wiper dies were made of heat-treated steel. The pressure and clamp die were made of cold work tool steels with a hardness scale of 55 Rockwell C. All of the dies, such as the bending, clamp, pressure and wiper dies were assembled with suitable interspaces. Then, the assembled dies were mounted on a bending machine.

In this research, the NC bending machine was used as shown in Fig. 7, with a bending radius of 25 to 250 mm and maximum angle of 195 degree.



Fig. 7. NC bending machine.

Also, the images of the dies were made and assembled on the bending system, which is shown in Fig. 8.

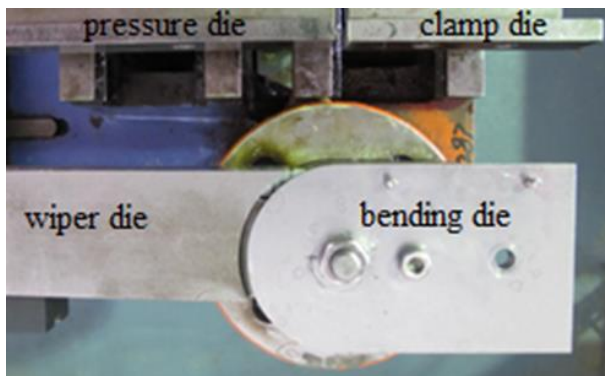


Fig. 8. Assembling dies on the bending system.

The thin wall cross section used in this study is 6010 aluminum alloy with a width of 31.64 mm, a height of 15.9 mm and a thickness of 1.6 mm with a bending radius of 25.4 mm in a 90-degree angle. The mechanical properties of the profile with a rectangular cross section and elasticity modulus of 69 GPa are the density of 2700 kg/m³ and Poisson ratio of 0.33. The uniaxial tension test (stress-strain) was obtained by cutting the uniaxial tension set sample with a width of 31.64 mm based on the ASTM E8M-04 standard. The results are shown in Fig. 9 in two modes of the experimental and power law stress-strain curves of AL6010-T6. According to Fig. 10, the experimental stress-strain curve can be curve fitted by the power law model using $K=225$ MPa and $n=0.25$.

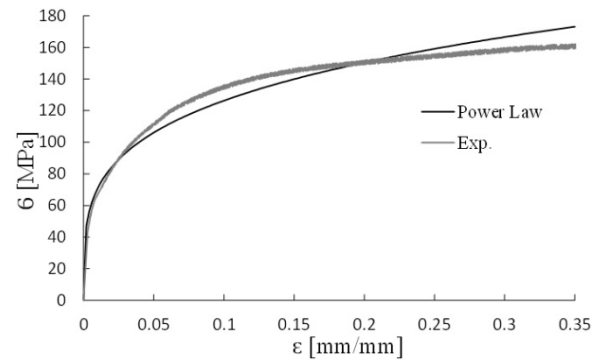


Fig. 9. Experimental and power law stress-strain curves of AL6010-T6.

According to Fig. 10 and Table 2, if R , H , and t stand, respectively, for the mean radius of the bend, the height of the profile and the thickness of the profile, the mandrel height – indicated with h – is obtained from Eq. (1). C represents the amount of clearance. This value is considered to be about 0.2 mm based on the DIN7154 and H11/c11 standards.

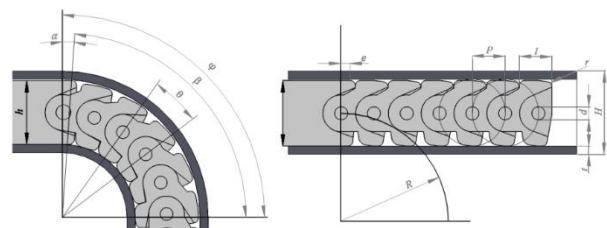


Fig. 10. (a) Bend angle parameters, (b) Geometrical die parameters.

One of the important parameters in the setting of the process is the mandrel pertusility, i.e. the position of the mandrel nose as far as the bend radius is concerned. This parameter affects the bending quality (e is shown in Fig. 11(b) and α angle is shown in Fig. 11(a)). In other words, the mandrel should be placed far enough ahead of the radius of the die in order to make sufficient pressure on the materials in the radius of the bend [2]. In this study, the value of e – as the forward position of the mandrel is shown in Fig. 11(b) – was extracted from a hypothetical triangle with one side as e , one side as the bending radius, and the third side was extracted as chord. The geometrical equation, number (2), was drawn from the Pythagorean law.

The minimum and maximum values were proposed in accordance with equations (3) and (4). In these equations, r is the bending radius of the mandrel's inner

edges. Therefore, the position of the mandrel depends on the bending radius, mandrel height, and the ratio of the profile height to the profile thickness. When the forward position of the mandrel was more than e_{max} , the profile interfered with the rectangular cross section of the mandrel, resulting in a very thin or cracked bend of the outer arch. Then, if it was less than e_{min} , the mandrel did not have sufficient pressure on the inner arch and led to wrinkling.

β as the effective angle of the mandrel cores was obtained by subtracting the bending angle (φ) from the protrusivity angle of the mandrel (α). It was obtained from Eq. (5). Considering the inclined circles which are bent in the profile canal, as can be seen in Fig. 11(b), P , the mandrel core's pitch, is obtainable from Eq. (6). θ is the corresponding angle of each mandrel core obtained from the radians in Eq. (7).

The core thickness (l) should be reasonable. If it is too small, the mechanical connection between the cores will be weak, and if it is thick, the clearance between the profiles and the cores will disappear, and the cores cannot bend up to the desired radius. Therefore, the core thickness at the top and bottom of the mean bend radius ought to be around the maximum and minimum values obtained from equations (8) and (9). The above-mentioned equations indicate that the core thickness from the pin to the top of the bend is fixed at l_{max} , so that the cores can be directly located and the core thickness from the middle pin to the down bend will be in a linear trend from l_{max} to l_{min} . Finally, n is the number of the calculated cores based on Eq. 10.

Table 2. The equation of the designed mandrel

No. Eq.	Equation	No. Eq.	Equation
1	$h = H - 2t - C$	6	$P \approx \frac{h}{2}$
2	$e^2 + \left(R + \frac{h}{2}\right)^2 = \left(R + \frac{H}{2} - t\right)^2$	7	$\theta \approx P / R$
3	$e_{max} = r + e$	8	$l_{max} = \theta R$
4	$e_{min} = r$	9	$l_{min} = \theta \left(R - \frac{h}{2}\right)$
5	$\beta = \varphi - \alpha = \varphi - \tan^{-1} \left(\frac{e}{R - \frac{H}{2} + t} \right)$	10	$n = \frac{R\beta}{l_{max}}$

The number of the existing geometric cores is considered to be eight cores. Therefore, by using the experimental data in this study, the output of the mandrel designs is presented in Table 3. The final design and assembly of the mandrels and core are shown in Fig. 11 and 12.

Table 3. The geometrical dimensions of the designed mandrel

parameter		parameter	
R [mm]	33.35	β [deg]	84
h [mm]	12.5	P [mm]	6.25
e [mm]	2.82	θ [rad]	10.7
φ [deg]	90	l_{min} [mm]	5.1
α [deg]	6	l_{max} [mm]	6.2

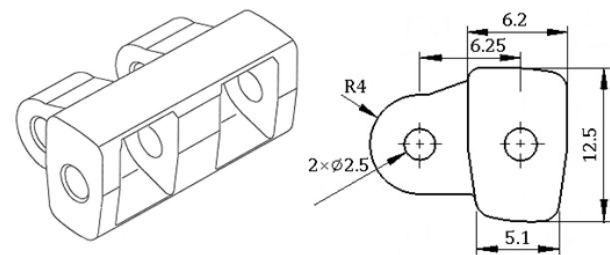


Fig. 11. The final design of the mandrel core.



Fig. 12. The newly designed mandrel along with the assembled cores.

The purpose of this study is to investigate how successful the process can be and the extraction of the strain distributions in order to investigate the defects of the process and improve the quality of the produced workpiece. Therefore, it is necessary to prepare the

samples before performing the experimental process. For this end, the four faces of the profile sections with rectangular cross sections were turned into grids, and the standard 2.5mm×2.5mm square grid was adopted with a laser machine with lines of 0.1 mm length. By measuring the previous grid dimensions and after conducting the bending process with the visual measurement system (VMS), the linear strain distributions were carried out with an accuracy of 0.01 mm. Also, for measuring the thick strain, the samples were cut after bending and the cross section thickness was calculated with a caliper with an accuracy of 0.01 mm. The thickness strain was measured by considering the first thickness. In this research, the experimental study was carried out in a constant temperature of 24°C, and in a constant angular velocity of 2.4 radians per minute. The linear velocity of the pressure die was considered to be the product of the angular velocity of the bending die in the mean bend radius. The value was calculated as 80 mm/min. In the RDB process, there are a lot of contacts between the dies and profiles. Frictional conditions are key factors in this process. Therefore, to achieve the appropriate frictional condition before the test, the die and profile surfaces should be cleaned and lubricated efficiently. For lubricating the mandrel and the inner surface of the profile, a special draw oil with the commercial code of S980B was used. To lubricate the external surface of the profile, an engine oil with a viscosity of 10 W was used. Also, due to the high friction needed between the clamp die and the rectangular cross section profile, the surface of the clamp die was roughened and not lubricated.

5. Results and Discussion

The results of the experimental study and the FEM simulation indicated that the material in the external arch of the bend did not have sufficient length extension ability and the profile was ruptured at this point. To fix this problem, the tested profiles should be placed under the annealing heat treatment to make them softer and have sufficient draw capability to complete the process. After the heat annealing process, the samples were prepared and experimented without any particular problems at 90-degree bending angle. This is shown in Fig. 13.



Fig. 13. Successful profile bending on the annealed heated rectangular cross sectional aluminum.

Then, after bending at a 45-degree angle, the engraving was measured in three internal, external, and side dimensions. Also, by measuring the bending profile (Fig. 14) the thickness changes were calculated. Therefore, the longitudinal strains (ϵ_L in the bending direction), width strains (ϵ_W , perpendicular to the bending direction) and thickness strains (ϵ_t in the thickness direction) were extracted at the bending angle of 45.

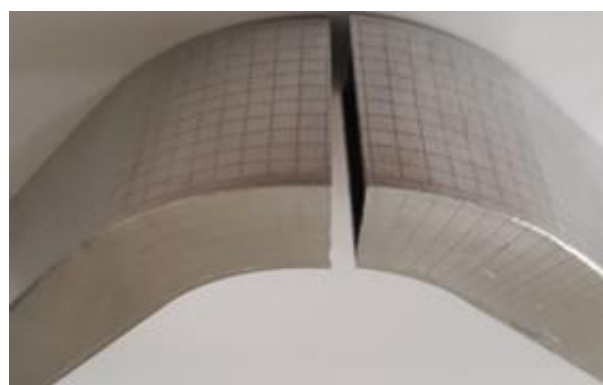


Fig. 14. Profile cut in 45-degree angle for measuring the thickness strain.

Moreover, the longitudinal and width strains of the internal and external dimensions (in the middle bends of the arch) were measured at different angles. The longitudinal and width strains of the sides were measured at different heights based on the bending arch and its angles.

The bending moment calculated from Eq. (20), $M = 131.66 N.m$, was compared to the bending moments extracted from the FEA as depicted in Fig. 15. The mean value of $M = 130.94 N.m$ was calculated from the FEA results. The results show good agreement.

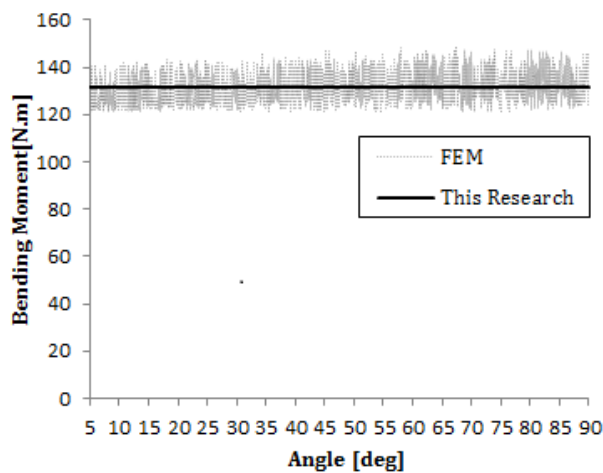


Fig. 15. bending moment versus the bend angle for the aluminum tube.

The position of the bending natural axis can be located wherever the sign of the circumferential strain on the lateral face of the bend is reversed. The analytical value of $\eta = 0.69$ calculated from Eq. (18) is in good agreement with $\eta = 0.7$ and $\eta = 0.71$ extracted from the experimental and FEA longitudinal strain distribution on the lateral face, respectively.

The major problem in RDB is the tearing of the external face of the bent. Therefore, the strain field on the external face of the bent plays a significant role in the prediction of tearing using the FLD diagrams, and the plane strain distribution in the transverse direction in the external face of the bent, as discussed previously, causes the use of only one point of the FLD diagram to predict tearing.

As Eq. (8) shows, the position of the bending natural axis affects the tangential strain in the external face of the bent. Therefore, accurate estimation of the position of the bending natural axis causes accurate strain distribution, and the possibility of tearing can be estimated more precisely. As Eq. (18) indicates, the position of the bending natural axis, η , depends on ρ , α , τ , and n and can be solved for various values of these parameters to draw a practical graph as depicted in Fig.

16. As this graph shows, the position of the bending natural axis tends to get close to the internal face of the bent as the bending radius decreases, and it tends to move to the center of the tube as the bending radius increases. Decreasing τ and n and increasing α cause the position of the bending natural axis to move toward the internal face of the bent.

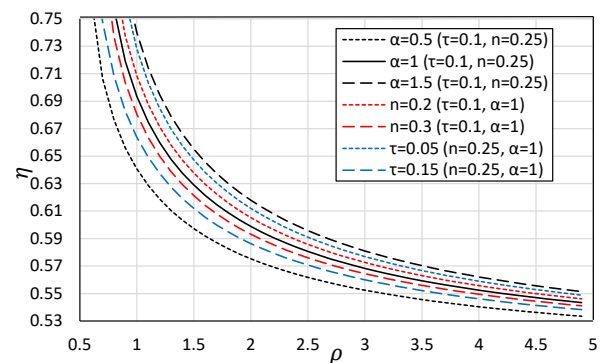


Fig. 16. A practical graph to predict the position of the bending natural axis (η).

In the experimental test, by measuring the final angle of the bend using the shadow graph and comparing it with the bending angle adjusted on the NC bending machine, the value of the spring back was measured experimentally as $\Delta\theta = 0.95$. The value of the analytical spring back was $\Delta\theta = 0.997$ using Eq. (25), whereas the value of $\Delta\theta = 0.98$ was extracted from the FEA, showing good agreement.

Radial (thickness), tangential (longitudinal), and axial (transverse) strains calculated from the analytical equations ((8) and (5)) and those extracted from the FEA and experimental test are depicted in Fig. 17 for the external faces of the bent. The angle is 45 degrees as shown in Fig. 17. In Fig. 18, the strains are placed in the middle of the cross section. The results indicated that the width strain was almost near zero, and the external side's draw of the bend in the direction of the bending caused the thickness to decrease. Due to the presence of the mandrel cores inside the profile and the small clearance between these cores and the profile, with the external side's draw, the material tended to shrink in width and thickness. Due to the presence of the mandrels, the material shrank in width only as much as the clearance between the core and the profile, and the predominant deformation was done in the thickness direction.

Therefore, the width strain was negative and close to zero. Thickness strains were done in the direction of negative and they were equal to the longitudinal strains. At the primary and end angles, the strain was lower and at the bending angle of 45, the greatest amount of the strains occurred as a result of the draw. The numerical and experimental results, while having a relatively good consistency, represented this physical argument. On the other hand, due to the small thickness of the profile, in comparison with other dimensions, the bending stresses were insignificant in comparison with the membrane strains; therefore, the strains and stresses can be created in the external side which is known as the membrane strain. With this condition, the deformation field in the external arch bending was very similar to the deformation field in the plane strain in the width direction.

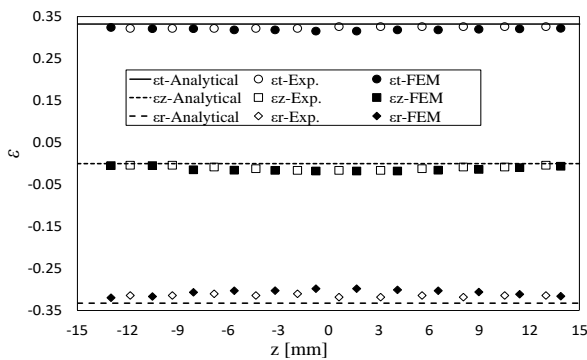


Fig. 17. Experimental, Analytical and Numerical strains in the external bend of the arch in a 45-degree angle.

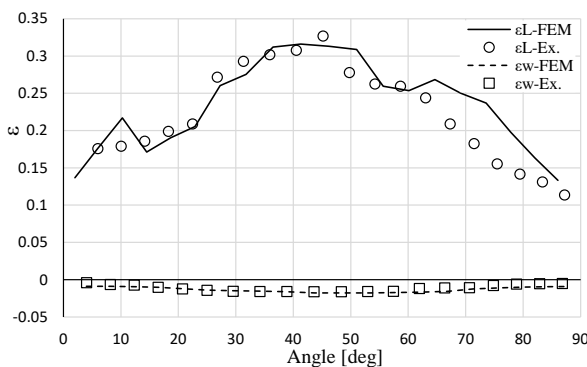


Fig. 18. Experimental and Numerical strains in the middle bend of the external arch.

Radial, tangential, and axial strains calculated from the analytical equations ((8) and (5)) and those extracted from the FEA and experimental test are depicted in Fig. 19 for the internal faces of the bend. The middle bending is indicated in Fig. 20. Here, the width strain was almost close to zero, and with compression in the internal arch,

the thickness increased in the direction of bending. Due to the presence of the mandrel cores inside the profile, and the small clearance between these cores and the profile, with compression in the internal arch, the material tended to draw (increase in dimensions) in the width and thickness directions. Depending on the die type, the material deform was very small in the width direction. But the predominant deformation was in the thickness direction. Therefore, in the width direction, the width strain was predicted to be close to zero. Thickness strains were done in the direction of positive and they were equal to the longitudinal strains. Also, the maximum amount of the strain occurred at a 45-degree angle. The strains were lower in the two sides of the bend. Numerical and experimental results, while having a relatively good consistency, represent this fact.

On the other hand, the comparison of the longitudinal strains of the external and internal sides of the bend (Fig. 17 and 19) show that the longitudinal strain in the external arch bend was about three times the size of the longitudinal strain in the internal arch bend. Therefore, it is expected that the position of the neutral axis is very close to the inside bend.

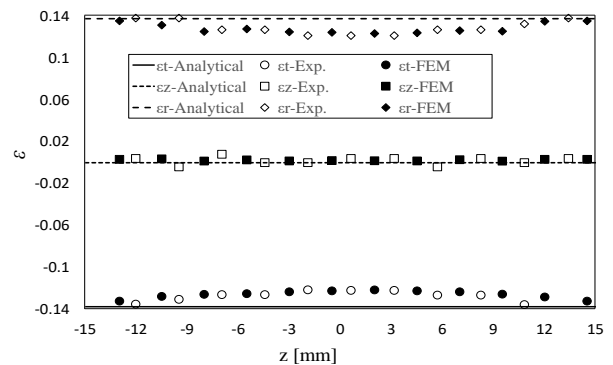


Fig. 19. Experimental, Analytical and Numerical strains in internal bend of the arch in a 45-degree angle.

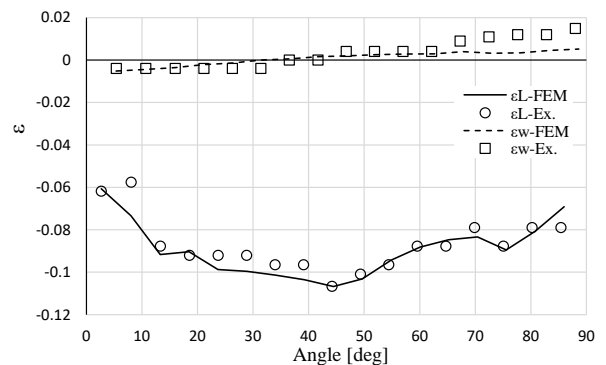


Fig. 20. Experimental and Numerical strains in the middle bend of the internal arch.

In addition, the radial, tangential, and axial strains of the lateral faces of the bend calculated from the analytical equations ((15) and (13)) and those extracted from the FEA and experimental test are depicted in Fig. 21 and 22. In this side, the longitudinal strain is tensile next to the external draw arch and it was compressed next to the internal draw arch. As mentioned before, the thickness of the external draw arch decreased and the thickness of the internal draw arch increased. Both arches came forward after the yield point and the difference in their longitudinal stresses is not noticeable in the plastic state. In order to balance the forces, it is necessary to move the neutral axis toward the thicker arch. For this reason, the neutral axis was close to the internal arch, which is indicated in Fig. 21 and 22. Also, at the bottom of the neutral axis, the longitudinal strain was in the compression form and the width strain was in the tensile form (at the bottom of the neutral axis, the height of the profile tended to increase), and at the top of the neutral axis, the longitudinal strain was in the tensile form and the width strain was in the compression form (at the top of the neutral axis, the height of the profile tended to decrease). Therefore, it is expected that the width strain size on the top and bottom sides of the bend be more than the corresponding size of the external and internal bend arches. This comparison is indicated in Fig. 17 to 22. As a result, the contribution of the thickness strain of the side deformation is less than its contribution to both the internal and external arches. In other words, at any point in the side of the bend, the thickness strain size was always less than the longitudinal strain size which is indicated in Fig. 21.

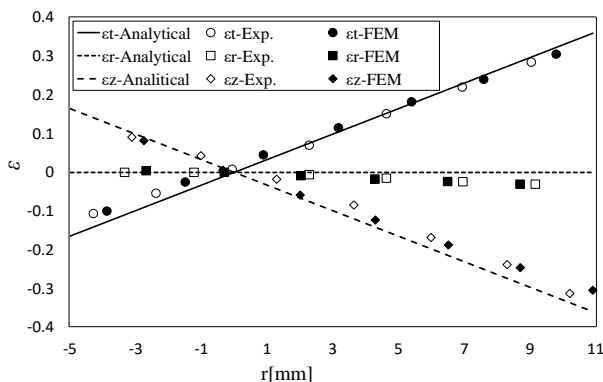


Fig. 21. Numerical, analytical and experimental strains in sides with a 45-degree angle.

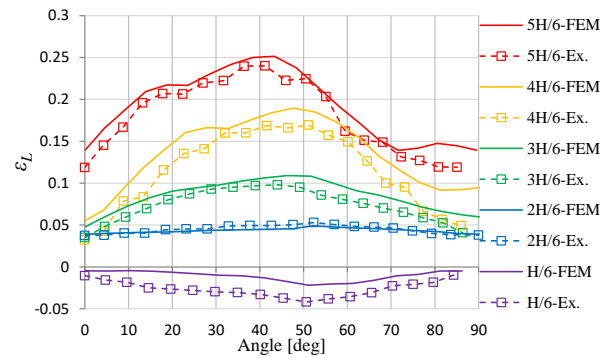


Fig. 22. The ratio of the numerical and experimental linear strains in the bend sides with different heights to the down side.

The comparison of the results, indicated in Fig. 17 to 22, shows good agreement, and neglecting the transverse strain in all faces of the bend is a correct assumption in the analytical analysis.

6. Conclusions

A new mandrel core geometry is developed in a rotary-draw bending process with a small bending radius. Some relationships were made for the proper design of the cores, based on which, new cores and mandrels were made and the process was successfully performed for annealed aluminum profiles with a small bending ratio of 1.6.

An analytical analysis of the rotary-draw bending process with a small bend radius for rectangular aluminum tube based on the power law hardening model was presented and accomplished experimentally. A 3D model of the tube and dies was constructed in ABAQUS commercial code, and the process was analyzed using the explicit finite element method. Experimental, analytical and FE outcomes of the analysis of the process show:

1- Due to the thinness of the rectangular tube and since the tube was enclosed by the dies and cores of the mandrel, the plane stress assumption in the thickness direction and the plane strain assumption in the transverse direction for all the faces of the tube can be used.

2- The thickness strain equaled the mines of the circumferential strain for the external and internal faces of the bent.

3- The position of the bending natural axis played a crucial role in distributing the strains and possibility of

tearing the external face of the bent predicted by the FLD diagrams.

4- Decreasing τ and n and increasing α caused the position of the bending natural axis to move toward the internal face of the bent.

5- The accurate bending moment predicted in this research can be used to select the proper machine for the bending process.

6- Rotary-draw bending process is a suitable process for bending thin walls with small bend radius. Mandrels and cores are used for maintaining the profile cross section while bending.

7- Suitable lubrication to reduce the friction coefficient has proved to be very successful in this process. In this research, S980B oil was used to carry out the process successfully.

8- One of the important parameters in the mandrel design is the proper positioning of the mandrels. If this value is lower or higher than the proposed limit, the process is doomed to failure.

9- The degree of the thickness reduction of the external bend is equal to the increase of the length. Therefore, the thickness increase of the arch bend is equal to the length reduction in the same side.

10- If the external bend ruptures, the annealing of the workpiece – due to the increased ductility – can be a good solution for the successful implementation of the process.

8. References

- [1] G. Y. Zhao, Y. L. Liu, Sh. Tian, H. Yang, Side wrinkling characteristics in rotary-draw bending process of thin-walled rectangular 3A21 tube, *Materials Science Forum* 697-698 (2012) 356-360.
- [2] J. T. Cmfege, Benedict, R. F. Veilleux, Tools and manufacturing engineer's handbook SME. Society of manufacturing engineers (SME), Michigan, (1984).
- [3] S. L. Semiatin, Metals handbook, ASM, Ohio-Metals Park, (1988).
- [4] K. X. Liu, Y. L. Liu, H. Yang, An analytical model for the collapsing deformation of thin-walled rectangular tube in rotary draw bending, *International Journal Advanced Manufacturing Technology* 69 (2013) 627-636.
- [5] G. Zhao, Y. Liu, R. Zhang, H. Yang, Optimal design of process parameters of rotary-draw bending process for thin-walled rectangular tube of aluminum alloy, *Journal of Engineering Manufacture* 228 (2014) 1442-1448.
- [6] G. Y. Zhao, Y. L. Liu, H. Yang, Numerical simulation on influence of clearance and friction on wrinkling in bending of aluminum alloy rectangular tubes, *Materials Science Forum* 546-549 (2007) 833-838.
- [7] G. Y. Zhao, Y. L. Liu, H. Yang, C. H. Lu, R. J. Gu, Three-dimensional finite-elements modeling of rotary-draw bending process for thin-walled rectangular tube, *Materials Science and Engineering* 499 (2009) 257-261.
- [8] K. Liu, Y. Liu, H. Yang, Experimental and FE simulation study on cross-section distortion of rectangular tube under multi-die constraints in rotary draw bending process, *International Journal of Precision Engineering and Manufacturing* 15 (2014) 633-641.
- [9] Sh. Tian, Y. Liu, H. Yang, Effects of geometrical parameters on wrinkling of thin-walled rectangular aluminum alloy wave-guide tubes in rotary-draw bending, *Chinese Journal of Aeronautics* 26 (2013) 242-248.
- [10] Z. Xing, Z. Xu, H. Yang, Ch. Lei, Numerical research on high-strength rectangular section steel tube in rotary-draw bending, *Key Engineering Materials* 620 (2014) 417-423.
- [11] H. Shen, Y. Liu, H. Qi, H. Yang, Sh. Zhou, Relations between the stress components and cross-sectional distortion of thin-walled rectangular waveguide tube in rotary draw bending process, *International Journal Advanced Manufacturing Technology* 68 (2013) 651-662.
- [12] F. Paulsen, T. Welo, O. P. Sovik, A design method for rectangular hollow sections in bending, *Journal of Materials Processing Technology* 113 (2001) 699-704.

تحلیل فرآیند خمکاری کششی دورانی برای پروفیل جدارنازک با مقطع مستطیلی آلومینیومی

سیدمحسن سیدحاتمی، حسین لکزیان

مجتمع دانشگاهی مواد و فناوری‌های ساخت، دانشگاه صنعتی مالک اشتر، تهران، ایران.

چکیده

فرآیند خمکاری کششی دورانی یا RDB روشی منحصر بفرد برای خمکاری شعاع‌های کوچک بوده که در حالت سرد برای خمکاری دقیق پروفیل‌های توخالی، توسط دستگاه‌های کنترل عددی NC انجام می‌شود. در این تحقیق یک مدل تحلیلی براساس مدل سخت‌شوندگی توانی برای فرآیند RDB روی پروفیل‌های جدارنازک با سطح مقطع مستطیلی ارائه می‌شود. بر اساس مقید بودن پروفیل در قالب‌ها و جدارنازک بودن آن، فرض تنش صفحه‌ای در راستای ضخامت و فرض کرنش صفحه‌ای در راستای عمود بر آن برای همه وجوه پروفیل استفاده می‌شود. با فرض تناسبی بودن فرآیند و قانون تئوری لوی - مایسز، میدان تنش پروفیل پیش‌بینی شده و با استفاده از تعادل نیروها در تمام وجوه پروفیل، موقعیت تار خنثی تعیین می‌شود. سپس گشتاور خم و مقدار برگشت فنری بصورت تحلیلی محاسبه می‌شود. با تحلیل هندسی پروفیل و فرآیند، یک مندرل جدید طراحی و ساخته شده و اجرا می‌شود. فرآیند با استفاده از حل صریح المان محدود در نرم افزار تجاری آباکوس مدل‌سازی و تحلیل شده و بصورت تجربی آزمایش می‌شود. مقایسه نتایج تحلیلی، عددی و تجربی روی میدان‌های کرنش، مطابقت خوبی را نمایش می‌دهد.

واژه‌های کلیدی: خمکاری کششی دورانی، مقاطع مستطیلی، حل تحلیلی، مدل سخت‌شوندگی توانی